

Nonlocal perimeter magnetoplasmons in a planar array of narrow quantum rings

Danhong Huang

Department of Physics, The University of Lethbridge, Lethbridge, Alberta, Canada T1K 3M4

Godfrey Gumbs

Department of Physics and Astronomy, Hunter College and the Graduate School, City University of New York, 695 Park Avenue, New York, New York 10021

(Received 23 October 1991)

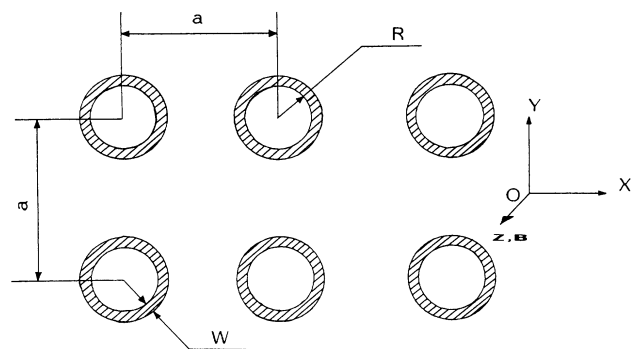
The collective excitations (perimeter magnetoplasmons) for a square-lattice array of quantum rings are calculated in the presence of a perpendicular magnetic field B . These calculations are done for thin rings whose width W is taken to be much smaller than the radius R and also satisfying $W \ll L_H$ where $L_H \equiv (\hbar c/eB)^{1/2}$ is the magnetic length. The Coulomb interaction between electrons produces a depolarization shift and also couples those transitions for which Δm is different, where Δm is the difference between the angular momentum quantum numbers for the initial and final states. This coupling induces a small gap between the Δm and $-\Delta m$ modes as well as a large gap between the states with different values of $|\Delta m|$. This gap decreases as $|\Delta m|$ increases. The collective excitation energies are also a periodic function of the magnetic flux $\Phi = \pi B R^2$ within a ring, with period equal to one flux quantum $\phi_0 = hc/e$. Only those excitations having the smallest difference $\pm \hbar$ in angular momentum have appreciable dispersion due to strong Coulomb interaction effects on them. There is a peak in the excitation energy spectrum for some value of the lattice constant a due to a competition between screening and the modification in the electron density. Moreover, there is an abrupt change in the slope of the dispersion curve as a function of $1/R^2$ when the magnetic flux Φ is either an integer or half-odd integer multiple of the flux quantum ϕ_0 .

I. INTRODUCTION AND SYNOPSIS

The outstanding achievements of semiconductor microfabrication technology have enabled researchers to carry out detailed investigations of electronic microstructures in spatially confined two-dimensional electron gas (2D EG) systems such as quantum wells, quantum wires and quantum dots. Quantum rings are another interesting low-dimensional electronic system which uniquely exhibit dimensionality crossover from zero to one dimension. It has been suggested in Ref. 1 that quantum rings may be fabricated with a technique that would use two gates having disk shapes, where one gate could form a quantum dot within the 2D EG and the other one would deplete the central region of the dot. There have already been several theoretical studies dealing with the ring geometry, e.g., perimeter magnetoplasmon,² Aharonov-Bohm oscillations,³ the eigenstates of two particles on a ring with magnetic flux,⁴ the effect of edge-channel scattering on the quantum electron transport in an annulus,⁵ as well as dynamic and coherent persistent currents in mesoscopic rings.^{6,7} In this paper, we calculate the electronic collective excitations for a square-lattice array of rings. This system is shown schematically in Fig. 1. In our notation, R is the radius of the ring, W is its width and a is the lattice constant of the square-lattice array. An ambient magnetic field B is applied perpendicular to the plane. There are two regimes of interest; one is the *thin-ring limit* and the other is the *wide-ring limit*. These two limits have several different features.

In the presence of a magnetic field, we require that both $W \ll R$ and $W \ll L_H$ are satisfied for thin rings. Here, $L_H \equiv (\hbar c/eB)^{1/2}$ is the magnetic length. For wide rings, we have $W \sim R$.

In this work, we restrict our attention to the thin-ring limit. This means that the energy-level separation for radial motion of the electrons is very large. Therefore, for thin rings, the radial motion is effectively frozen out, so that only the electron *angular* motion contributes to the



Planar Array of Quantum Rings

FIG. 1. Schematic representation of a planar array of quantum rings. Here, R is the radius of a ring, W is its width, and a is the lattice constant of the square lattice. A uniform magnetic field B is applied in the direction perpendicular to the 2D plane.

dynamical response. We will show below that the angular momentum quantum number m for the highest occupied energy level changes with magnetic field. Moreover, we have found that the screening function in the effective Coulomb interaction is independent of the strength of the magnetic field. The Coulomb interaction between electrons produces a depolarization shift and also couples those transitions for which Δm is different. Here, Δm denotes the difference between the angular momentum quantum numbers for the initial and final states. This coupling induces a small gap between the Δm and $-\Delta m$ modes as well as a large gap between the states with different values of $|\Delta m|$. This gap decreases as $|\Delta m|$ increases, which means that the single-particle contributions increasingly become more important for large values of $|\Delta m|$. The magnetoplasmon excitation energies clearly show *anticrossing* as a function of the magnetic field B . The magnitude of the gap between two modes produced by anticrossing gives one a sense of the effects due to the Coulomb coupling on these modes. The collective modes are also a periodic function of the magnetic flux $\Phi = \pi BR^2$ within a ring, with period equal to one flux quantum $\phi_0 = hc/e$. Due to nonlocal effects, the quantum magnetoplasmons have dispersion as a function of the wave vector in both the x and y directions. The dispersion in these two directions is also periodic, with period equal to the reciprocal-lattice vector $G = 2\pi/a$. This may be interpreted as being due to the square-lattice structure within the plane. Only those modes having the smallest difference $\pm\hbar$ in angular momentum have appreciable dispersion due to strong Coulomb interaction effects on them. When the lattice constant a is large, the depolarization shift is negligible because of a decrease in the average two-dimensional electron density n_{2D} which is proportional to $1/a^2$. Moreover, the Coulomb interaction between electrons on different rings decreases with a , for sufficiently large a . As a result, the excitation energy spectrum of the collective modes could be well approximated by ignoring the Coulomb interaction and using the energy eigenvalues of a single particle on a ring. Therefore, the excitation energy decreases as a increases. On the other hand, when a is reduced, the screening is appreciable although n_{2D} is increased. Therefore, the excitation energy again decreases in the limit of small a as the lattice constant is reduced. In our numerical calculations, we have found a peak in the excitation energy spectrum for some value of the lattice constant a due to

a competition between screening and a modification in the electron density. Our calculations show that when the radius of the ring R is small, the excitation energy is a linear function of $1/R^2$ since the single-particle kinetic energy is so large that it dominates the small Coulomb interaction between electrons. This reproduces the single-particle-like feature on a ring in the excitation spectrum. When R is large, the single-particle kinetic energy and the Coulomb interaction are comparable. In this limit, the oscillations of the excitation energy as the magnetic flux Φ varies have been calculated as a function of R . For this, B is fixed and Φ changes with R . This produces an abrupt change in the slope of the dispersion curve as a function of $1/R^2$ when the magnetic flux Φ is either an integer or half-odd integer multiple of the flux quantum ϕ_0 . When R is further increased, the “kinks” gradually develop into maxima and minima. The amplitude of the oscillations of the magnetoplasmon energies increases due to the quenching of the single-particle kinetic energy. In this regime, the Coulomb interaction becomes considerably more important and leads to significant shifts in the locations of the maxima and minima away from their positions that correspond to flux quantization. This ensures that flux quantization effects cannot be ignored in this case.

The rest of this paper is organized as follows. In Sec. II, we derive the dispersion relation for a square-lattice array of quantum rings. In our model, we include the infinitesimal but finite thickness of the 2D EG inversion layer. In Sec. III, we present numerical results for the single-particle energy and the perimeter magnetoplasmon excitation energies as functions of magnetic field, wave vector, lattice constant, and the radius of the ring.

II. MODEL FOR QUANTUM RINGS AND FORMALISM

In this section, we derive the dispersion relation for plasma oscillations in the random-phase approximation (RPA) when a uniform magnetic field \mathbf{B} is applied perpendicular to the array of narrow quantum rings. To formulate the problem mathematically, let the plane containing the rings coincide with the xy plane, and let the magnetic field be parallel to the z axis. The Hamiltonian for an electron of effective mass m^* on a ring is, making use of the symmetric gauge $\mathbf{A} = \frac{1}{2}\mathbf{B} \times \mathbf{r}$ for the vector potential, given by²

$$\mathcal{H} = -\frac{\hbar^2}{2m^*} \left[\frac{1}{\rho} \frac{d}{d\rho} \left(\rho \frac{d}{d\rho} \right) + \frac{1}{\rho^2} \frac{d^2}{d\phi^2} + \frac{d^2}{dz^2} \right] - \frac{ie\hbar B}{2m^*c} \frac{d}{d\phi} + \frac{e^2 B^2 \rho^2}{8m^*c^2} + V_{\text{eff}}(\rho) + U_{\text{eff}}(z). \quad (1)$$

Here, ρ, ϕ, z are cylindrical polar coordinates of an electron and $V_{\text{eff}}(\rho), U_{\text{eff}}(z)$ represent the effective potential in the radial and axial directions, respectively. The single-particle eigenstates for an isolated ring are²

$$\Psi_{n,m}^{(s)}(\rho, \phi) \xi_0(z) = \frac{e^{im\phi}}{\sqrt{2\pi}} R_{n,m}(\rho) \xi_0(z), \quad (2)$$

where $R_{n,m}(\rho)$ is the radial wave function for electron

motion in the effective potential $V_{\text{eff}}(\rho)$. Also, n ($= 1, 2, 3, \dots$) and m ($= 0, \pm 1, \pm 2, \dots$) are the radial and angular momentum quantum numbers, respectively. $\xi_0(z)$ is an axial electron wave function, representing the quantum confinement at the heterojunction for $z \geq 0$.

We now consider a square-lattice array of quantum

$$|\nu\rangle = |k_x, k_y; n, m\rangle = \frac{\xi_0(z)}{(N_x N_y)^{1/2}} \sum_{j, j'} \exp \left[i k_x j a + i k_y j' a - i \left(\frac{e}{\hbar c} \right) \mathbf{A} \cdot \mathbf{R}_{j, j'} \right] \Psi_{n, m}^{(s)}(\rho - \mathbf{R}_{j, j'}), \quad (3)$$

where $\mathbf{R}_{j, j'} = (j\hat{\mathbf{e}}_x + j'\hat{\mathbf{e}}_y)a$ is a 2D lattice vector. We assume that there are $(N_x \times N_y)$ rings on the plane, with periodic boundary conditions. We take $\xi_0(z)$ as a variational wave function of the form⁸

$$\xi_0(z) = \frac{1}{\sqrt{2L_z^3}} z e^{-z/2L_z} \quad \text{for } z \geq 0 \quad (4)$$

and is zero for $z < 0$. L_z is the thickness of the 2D layer. In our model, we assume that the electrons are in the lowest energy level associated with confinement in the z direction since the confining potential in this direction is strong.

We now include the many-body effects due to the Coulomb interaction between electrons on the same ring and on different rings. When an external potential of the form

$$V^{\text{ext}}(\rho; t) = V^{\text{ext}}(q_x, q_y; \omega) e^{i[\omega t - (q_x x + q_y y)]} \quad (5)$$

is applied, the perturbation in the electron density induces a Hartree and exchange-correlation potential. In this paper, we only include the Hartree self-consistent-field potential since the contribution due to exchange and

rings, shown schematically in Fig. 1. We take account of the screening due to the background medium by assuming that the array is immersed in a material with effective dielectric constant ϵ_s . The single-particle Bloch wave functions for the ring array have the periodicity of the lattice and are given by

correlation produces a small correction. These effects could be incorporated into our calculation with the use of the local-density approximation (LDA).⁹ The induced Hartree potential is a solution of Poisson's equation

$$V^H(q_{xy}; z) = \frac{2\pi e^2}{\epsilon_s q_{xy}} \int dz' e^{-q_{xy}|z-z'|} \delta n(q_{xy}; z'), \quad (6)$$

where $q_{xy} = (q_x^2 + q_y^2)^{1/2}$, and the induced electron density in linear-response theory is given by¹⁰

$$\delta n(q_{xy}; z) = |\xi_0(z)|^2 \sum_{\nu, \nu'} \langle \nu | V^{\text{tot}}(\rho') | \nu' \rangle \times \langle \nu' | \exp(i\mathbf{q} \cdot \rho') | \nu' \rangle \times \frac{f_0(E_\nu) - f_0(E_{\nu'})}{\hbar\omega - (E_{\nu'} - E_\nu)}, \quad (7)$$

where ν is a composite index for the electron eigenstates, $f_0(E)$ is the Fermi-Dirac statistical function, and E_ν is the single-particle energy. Also, $V^{\text{tot}} = V^{\text{ext}} + V^H$ is the total perturbation.

Equations (6) and (7) jointly give

$$V^H(q_{xy}) \equiv \int dz V^H(q_{xy}; z) |\xi_0(z)|^2 = \frac{2\pi e^2}{\epsilon_s q_{xy}} I(q_{xy}) \sum_{\nu, \nu'} \sum_{\mathbf{q}'} V^{\text{tot}}(\mathbf{q}') \langle \nu | \exp(-i\mathbf{q}' \cdot \rho') | \nu' \rangle \langle \nu' | \exp(i\mathbf{q} \cdot \rho') | \nu \rangle \frac{f_0(E_\nu) - f_0(E_{\nu'})}{\hbar\omega - (E_{\nu'} - E_\nu)}, \quad (8)$$

where the screening factor, due to the finite thickness of the 2D layer, is⁸

$$I(q_{xy}) = \int dz \int dz' |\xi_0(z)|^2 |\xi_0(z')|^2 e^{-q_{xy}|z-z'|} = \frac{8 + 9q_{xy}L_z + 3(q_{xy}L_z)^2}{8(1 + q_{xy}L_z)^3}. \quad (9)$$

For the tight-binding wave function in Eq. (3), the matrix elements in Eq. (8) have been calculated as

$$\langle \nu' | \exp(i\mathbf{q} \cdot \boldsymbol{\rho}') | \nu \rangle = \delta(k'_x - k_x - q_x - lG) \delta(k'_y - k_y - q_y - l'G) A_{n',m';n,m}(\mathbf{q}), \quad (10)$$

where $G = 2\pi/a$ is a reciprocal-lattice vector and $l, l' = 0, \pm 1, \pm 2, \dots$ include the effects due to umklapp scattering. The form factor is defined by

$$A_{n',m';n,m}(\mathbf{q}) = \int d^2 \boldsymbol{\rho}' e^{i\mathbf{q} \cdot \boldsymbol{\rho}'} \Psi_{n',m'}^{*(s)}(\boldsymbol{\rho}') \Psi_{n,m}^{(s)}(\boldsymbol{\rho}'), \quad (11)$$

where $\Psi_{n,m}^{(s)}(\boldsymbol{\rho}')$ is the single-particle eigenfunction given in Eq. (2). The modes of collective excitation are determined from the self-sustaining condition, which corresponds to setting $V^{\text{ext}} = 0$. Substituting Eq. (10) into Eq. (8), a straightforward calculation gives

$$V^H(|\mathbf{q} + \mathbf{G}_{l,l'}|) = U(|\mathbf{q} + \mathbf{G}_{l,l'}|) \sum_{n',m'} \sum_{n,m} \Pi_{n',m';n,m}(\omega) A_{n',m';n,m}(\mathbf{q} + \mathbf{G}_{l,l'}) \times \left[\sum_{j,j'} V^H(|\mathbf{q} + \mathbf{G}_{j,j'}|) A_{n',m';n,m}^*(\mathbf{q} + \mathbf{G}_{j,j'}) \right], \quad (12)$$

where the Fourier transform of the Coulomb potential is

$$U(q_{xy}) = \frac{2\pi e^2}{\epsilon_s q_{xy}} I(q_{xy}), \quad (13)$$

and $|\mathbf{q} + \mathbf{G}_{j,j'}| = [(q_x + jG)^2 + (q_y + j'G)^2]^{1/2}$. The polarization function $\Pi_{n',m';n,m}(\omega)$ is given by

$$\Pi_{n',m';n,m}(\omega) = \frac{f_0(E_{n,m}) - f_0(E_{n',m'})}{\hbar\omega - (E_{n',m'} - E_{n,m})}. \quad (14)$$

The solutions corresponding to Eq. (12) can be obtained by solving the following secular equation:

$$\text{Det} \left[\delta_{n',m';s',t'} \delta_{n,m;s,t} - \Pi_{n',m';n,m}(\omega) \sum_{j,j'} U(|\mathbf{q} + \mathbf{G}_{j,j'}|) A_{n',m';n,m}(\mathbf{q} + \mathbf{G}_{j,j'}) A_{s',t';s,t}^*(\mathbf{q} + \mathbf{G}_{j,j'}) \right] = 0. \quad (15)$$

Since we are only concerned with the thin-ring limit ($W \ll R$ and $W \ll L_H$), we approximate the electron-density profile in the radial direction by the Dirac δ function¹¹

$$|R_{n,m}(\rho)|^2 = \frac{1}{\rho} \delta(\rho - R). \quad (16)$$

This means that only those transitions between energy eigenstates with the same radial quantum number and different angular momentum quantum numbers are allowed. With this simplifying assumption, the single-particle energy levels are

$$E_m = \frac{m^* R^2}{8\hbar^2} \left[\hbar\omega_c + \frac{2m\hbar^2}{m^* R^2} \right]^2, \quad (17)$$

where $\omega_c = eB/m^*c$ is the Larmor frequency. The energy eigenvalues in Eq. (17) are shown in Fig. 2. It is clear that the angular momentum quantum number for the highest occupied state varies with the magnetic flux Φ inside the ring. These changes in the quantum number occur at the points of intersection of the single-particle energy levels plotted in Fig. 2. In this approximation, the dispersion relation in Eq. (15) is simplified and the result is

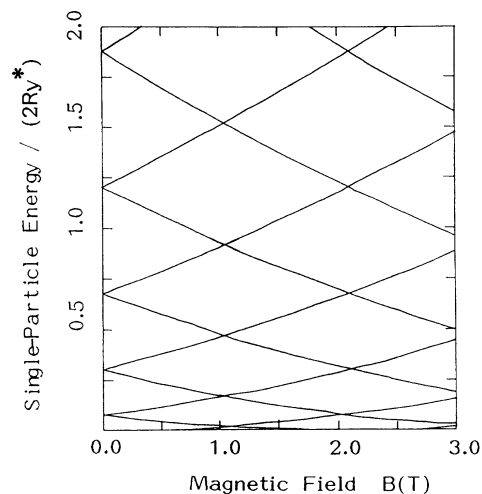


FIG. 2. Calculated single-particle energy spectrum as a function of magnetic field B . Here, $2Ry^* = \hbar^2/(m^*a_B^2) = 11.66$ meV is the energy scale. The parameters used in the calculation are $m^* = 0.067m_e$, $R = 2.58a_B^*$, where $a_B^* = \hbar^2\epsilon_s/m^*e^2 = 97.01$ Å is the length scale. The levels can be labeled by the angular momentum quantum number m . Eleven energy levels around $B = 0$, from the lowest to the highest, are labeled by $m = 0, \pm 1, \pm 2, \dots, \pm 5$, respectively.

$$\text{Det} \left[\delta_{\Delta m, \Delta t} - \chi_{\Delta m, 0}(\omega) \sum_{j, j'} U(|\mathbf{q} + \mathbf{G}_{j, j'}|) A_{\Delta m, 0}(\mathbf{q} + \mathbf{G}_{j, j'}) A_{\Delta t, 0}^*(\mathbf{q} + \mathbf{G}_{j, j'}) \right] = 0. \quad (18)$$

where Δm and Δt ($= \pm 1, \pm 2, \dots$) stand for the changes of angular momenta for the transitions between initial and final states. Also, the form factor in Eq. (18) is

$$A_{\Delta m, 0}(\mathbf{q}) \equiv \frac{1}{2\pi} \int_0^{2\pi} d\phi e^{-i\Delta m\phi} e^{i\mathbf{q}\cdot\mathbf{R}} \\ = [1 - \delta(|\mathbf{q}|)] (i)^{|\Delta m|} e^{-i\Delta m\theta(\mathbf{q})} J_{|\Delta m|}(|\mathbf{q}|R) \quad (19)$$

where $J_m(x)$ is a Bessel function of the first kind and the irreducible polarizability at zero temperature is

$$\chi_{\Delta m, 0}(\omega) = \frac{1}{2} \sum_m \left[\frac{n_m - n_{m+\Delta m}}{\hbar\omega - (E_{m+\Delta m} - E_m)} + \frac{n_m - n_{m-\Delta m}}{\hbar\omega - (E_m - E_{m-\Delta m})} \right]. \quad (20)$$

In our notation, n_m is the average areal density of energy level m and we define the function $\theta(\mathbf{q})$ in Eq. (19) by

$$\theta(\mathbf{q}) = \begin{cases} \tan^{-1}\left(\frac{q_y}{q_x}\right) & \text{if } q_x > 0 \\ \frac{\pi}{2} \text{sgn}(q_y) & \text{if } q_x = 0 \\ \pi + \tan^{-1}\left(\frac{q_y}{q_x}\right) & \text{if } q_x < 0, \end{cases} \quad (21)$$

where $\text{sgn}(x)$ is the standard sign function. In contrast to previous work,² our calculations show that only the global lattice symmetry is retained for the quantum ring array. Therefore, the collective excitations may be classified by their wave vectors $\mathbf{q} = (q_x, q_y)$. The modes are periodic in the x and y directions with period $G = 2\pi/a$. The perimeter magnetoplasmon modes with different Δm are coupled to each other. In Ref. 2, the local circular symmetry for the ring superlattice has

$$a = 10.0a_B^*, \quad L_z = 0.52a_B^*, \quad R = 2.58a_B^*, \quad q_x = q_y = \frac{\pi}{2a}, \quad B = 1.0 \text{ T}.$$

Here, $a_B^* \equiv \hbar^2 \epsilon_s / m^* e^2 = 97.01 \text{ \AA}$ and $2 \text{ Ry}^* \equiv \hbar^2 / (m^* a_B^{*2}) = 11.66 \text{ meV}$ are the effective Bohr radius and twice the effective Rydberg energy, respectively. These are the length and energy scales used in all the figures. The arrows in Fig. 3 indicate the positions of the zeros of the determinant. These correspond to the excitation energies of the perimeter magnetoplasmon modes. The four vertical straight lines in the figure are located where the determinant has singularities which are at the single-particle energies.

It is instructive to compare the single-particle energy in Fig. 2 plotted as a function of magnetic field with the B

been maintained. Therefore, the collective excitations have been classified by the change in angular momentum. The coupling between these modes has been excluded. For simplifying our calculations, we have assumed that there are two electrons on each ring. This means that only the lowest energy level is occupied.⁹ Although this is a simplification, we believe that the qualitative features obtained in our calculations would not be affected when more than one level is occupied. For this simple model, we have

$$n_m = \begin{cases} 0 & \text{if } m > 0 \\ 2a^{-2} & \text{if } (2|m| - 1) < \frac{\Phi}{\phi_0} < (2|m| + 1) \\ a^{-2} & \text{if } \frac{\Phi}{\phi_0} = (2|m| \pm 1). \end{cases} \quad (22)$$

A detailed investigation with numerical results of perimeter magnetoplasmon excitation energies as functions of magnetic field, wave vector, lattice constant, and radius of the ring is presented in the next section.

III. NUMERICAL RESULTS

Figure 3 is a plot of the determinant of the dielectric matrix defined by Eq. (18). Since we are primarily interested in the low-energy magnetoplasmon modes, we have truncated this determinant into a (4×4) determinant. This means that only the modes with $\Delta m = \pm 1, \pm 2$ are included. In our calculations, we have used the following parameters:

$$\epsilon_s = 12.5, \quad m^* = 0.067m_e,$$

where m_e is the bare electron mass and

dispersions of perimeter magnetoplasmon modes in Fig. 4. The four curves, from the lowest to the highest one, represent the coupled modes with $\Delta m = -1, +1, -2, +2$, respectively. The parameters used in the calculation are the same as in Fig. 3, except that the magnetic field varies here. The results in Fig. 4 show that whenever the magnetic flux $\Phi = \pi BR^2$ inside the ring is an integer multiple of the flux quantum $\phi_0 = hc/e$, there is a small gap between the Δm and $-\Delta m$ modes due to the coupling between them. On the other hand, whenever the magnetic flux Φ is a half-odd integer times the flux quantum ϕ_0 , there is a large gap between the Δm and

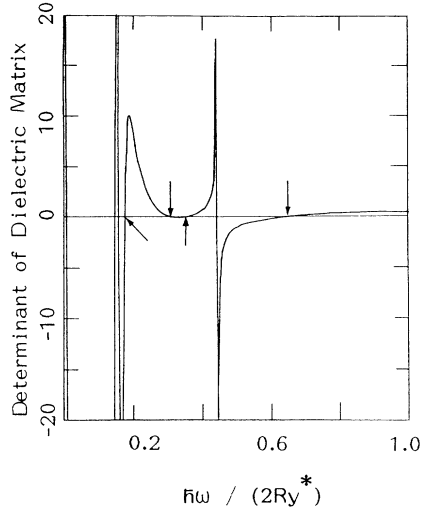


FIG. 3. The curve for the determinant of the dielectric matrix as a function of energy. The energy is in units of 2 Ry^* . The parameters used in the calculation are $\epsilon_s = 12.5$, $m^* = 0.067m_e$, $a = 10.0 a_B^*$, $L_z = 0.52 a_B^*$, $R = 2.58 a_B^*$, $q_x = q_y = \pi/2a$, and $B = 1.0 \text{ T}$. The four arrows indicate the zeros of the determinant, corresponding to the energies of the magnetoplasmon modes. The four vertical straight lines denote the positions of the singularities of the determinant, corresponding to the single-particle energies.

$-(\Delta m + 1)$ modes due to the Coulomb coupling. This gap decreases as $|\Delta m|$ increases, indicating that in this limit the Coulomb coupling becomes more and more important. The dispersion curve clearly shows anticrossing. The magnitude of the gap between the magnetoplasmon modes produced by anticrossing is a measure of the effects due to the Coulomb coupling on these modes. The

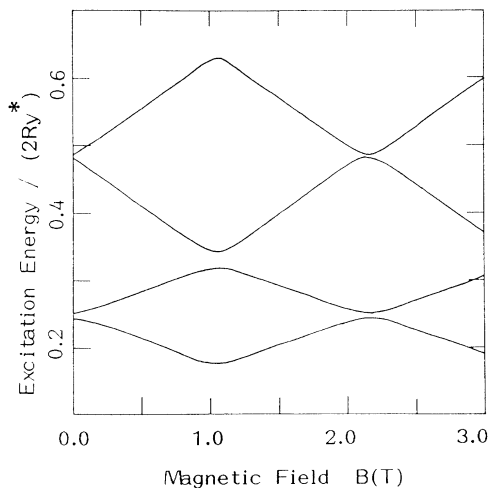


FIG. 4. The perimeter magnetoplasmon modes for $\Delta m = \pm 1, \pm 2$ as a function of magnetic field. Energy is measured in units of 2 Ry^* . The parameters used in the calculation are $\epsilon_s = 12.5$, $m^* = 0.067m_e$, $a = 10.0 a_B^*$, $L_z = 0.52 a_B^*$, $R = 2.58 a_B^*$, and $q_x = q_y = \pi/2a$. The four modes, from the lowest to the highest, are related to the transition with $\Delta m = -1, +1, -2, +2$, respectively.

excitation energy of the magnetoplasmons is a periodic function of the magnetic flux Φ with period equal to ϕ_0 . By comparing the single-particle spectrum in Fig. 2 with Fig. 4, it is clear that the depolarization shift is not negligible.

Figure 5 is a plot of the excitation energies of the magnetoplasmon modes for $\Delta m = 1$ and $\Delta m = -1$ as a function of wave vector. Here, the parameters used in the calculation are the same as those in Fig. 3, except that q_x and q_y are varying. The points Γ , X , and M in Fig. 5 are defined as the following three symmetric points in wave-vector space: $(q_x, q_y) = (0, 0)$, $(\frac{\pi}{a}, 0)$, $(\frac{\pi}{a}, \frac{\pi}{a})$, respectively. The magnetoplasmon dispersion in both the x and y directions is periodic, with period equal to the reciprocal-lattice vector $G = 2\pi/a$. This is a consequence of the square-lattice structure within the plane. However, the dispersion relation from Γ to X and Γ to M is asymmetric. This implies that only the global lattice symmetry is retained for the quantum ring array, while the local circular symmetry of a single ring is lost. Therefore, the collective excitations could be classified according to their wave vectors q_x and q_y and modes with different Δm are coupled to each other. In contrast, Ref. 2 showed that the local circular symmetry for a ring superlattice is maintained. Therefore, the excitations have been classified by the value of Δm . Furthermore, we have found that only modes with $\Delta m = \pm 1$ have appreciable dispersion as a result of the strong nonlocal Coulomb interaction between electrons. This confirms that perimeter magnetoplasmons with large $|\Delta m|$ possess more single-particle contributions. For the $\Delta m = 1$ mode, the dispersion for the excitations between X and M is weak, but the dispersion for the $\Delta m = -1$ mode is strong. Also, the asymmetry from Γ to X and Γ to M is stronger for this mode.

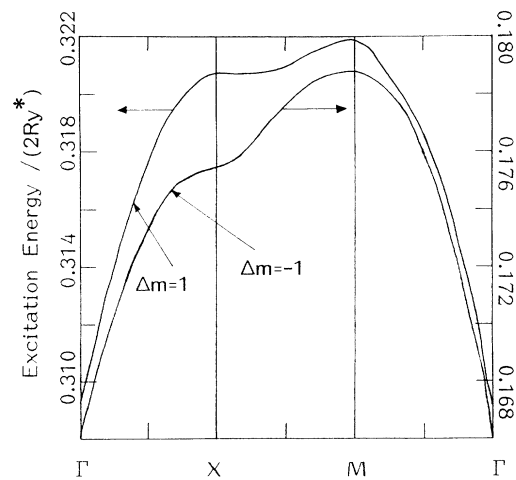


FIG. 5. The wave-vector dispersion for perimeter magnetoplasmon modes with $\Delta m = \pm 1$. The energy is in units of 2 Ry^* . The parameters used in the calculation are $\epsilon_s = 12.5$, $m^* = 0.067m_e$, $a = 10.0 a_B^*$, $L_z = 0.52 a_B^*$, $R = 2.58 a_B^*$, and $B = 1.0 \text{ T}$. The symbols Γ , X , and M correspond to the points $(q_x, q_y) = (0, 0)$, $(0, \frac{\pi}{a})$, and $(\frac{\pi}{a}, \frac{\pi}{a})$ in wave-vector space.

Figure 6 shows plots of the excitation energies as a function of the lattice constant a for the $\Delta m = 1$ and $\Delta m = -1$ modes. In our calculations, the parameters are the same as those in Fig. 3, but here the lattice constant a is varying. In the limit that a becomes large, both the Coulomb coupling and the depolarization shift are negligible because of a decrease in the average two-dimensional electron density $n_{2D} = 2/a^2$. Furthermore, for this range of density, the Coulomb interaction between electrons on different rings decreases as a increases. Therefore, for sufficiently large a the excitation energy decreases as a increases. As a result, the excitation energy spectrum could be well described by the energy eigenvalues of one electron on a ring. However, when a is reduced, the screening greatly increases although n_{2D} is increased also. This can be clearly seen from the reductions of the form factor $A(\mathbf{q} + \mathbf{G}_{j,j'})$ and the Coulomb potential $U(|\mathbf{q} + \mathbf{G}_{j,j'}|)$ in Eq. (18) for fixed \mathbf{q} as a increases. Therefore, the excitation energy again decreases in the limit of small a as the lattice constant is reduced. In our calculations, we have found a peak in the excitation energy spectrum for a value of the lattice constant a due to a competition between screening and the changes in the electron density. The energy of the perimeter magnetoplasmons as a function of the radius R of a ring is shown in Fig. 7, for the $\Delta m = \pm 1$ modes, respectively. All the parameters in the calculation are the same as those used in Fig. 3, except that R is varying. When the radius of the ring R is small, the excitation energy is a linear function of $1/R^2$ since the single-particle kinetic energy is so large that it dominates the small Coulomb interaction between electrons. This results in the single-particle-like behavior in the excitation spectrum for small values of R . As R becomes large, the single-particle kinetic energy and the Coulomb inter-

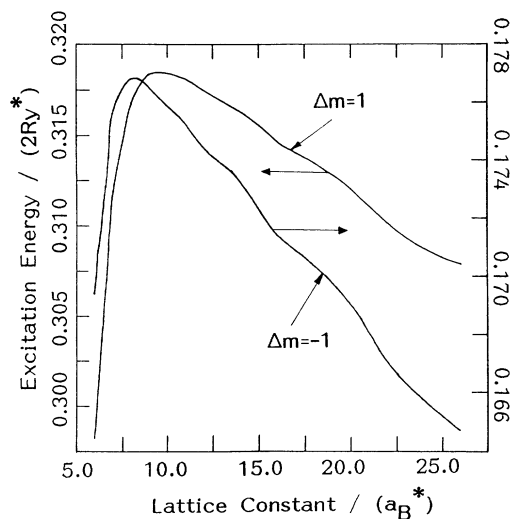


FIG. 6. The perimeter magnetoplasmon excitation energy as a function of the lattice constant a for $\Delta m = \pm 1$. The energy is in units of 2 Ry^* , and the lattice constant a is in units of a_B^* . The parameters chosen in the calculation are $\epsilon_s = 12.5$, $m^* = 0.067m_e$, $L_z = 0.52a_B^*$, $R = 2.58a_B^*$, $q_x = q_y = \pi/2a$, and $B = 1.0 \text{ T}$.

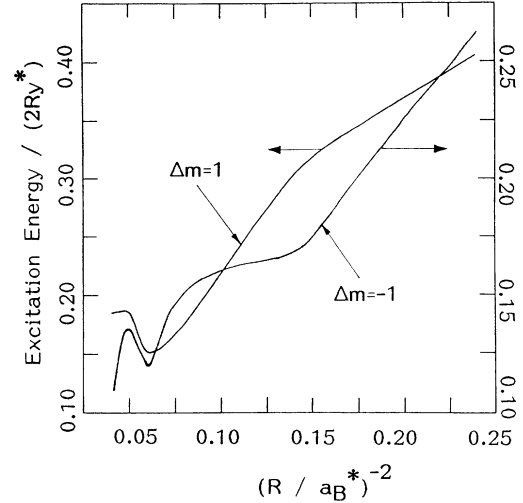


FIG. 7. The perimeter magnetoplasmon excitation energy as a function of $1/R^2$ for $\Delta m = \pm 1$, where R is the radius of the ring. The energy is in units of 2 Ry^* , and the radius R is measured in units of a_B^* . The parameters used in the calculation are $\epsilon_s = 12.5$, $m^* = 0.067m_e$, $a = 10.0 a_B^*$, $L_z = 0.52 a_B^*$, $q_x = q_y = \pi/2a$, and $B = 1.0 \text{ T}$.

action are comparable. The oscillations of the excitation energy as a function of the magnetic flux Φ have been calculated as a function of R . Here, the magnetic field is fixed and the flux changes with R . This produces an abrupt change in the slope of the dispersion curves as a function of $1/R^2$ when the magnetic flux Φ is either an integer or half-odd integer multiple of the flux quantum $\phi_0 = hc/e$. Whenever the slope increases abruptly for the $\Delta m = 1$ mode, the slope for the $\Delta m = -1$ mode is decreased for increasing R . When R further increases, these “kinks” gradually develop into well-defined maxima and minima. The amplitude of the oscillations in the dispersion curve is enhanced because of the quenching of the single-particle kinetic energy. In this case, the Coulomb interaction becomes more important and leads to significant shifts in the locations of the maxima and minima away from the positions that correspond to flux quantization.

IV. CONCLUDING REMARKS

In summary, we have calculated the excitation energies of perimeter magnetoplasmons in a 2D array of narrow quantum rings. We have computed the single-particle energies as well as the collective excitation energies as a function of magnetic-field strength. The effect due to magnetic flux quantization on the magnetoplasmon modes corresponds to the oscillations as the magnetic field varies. Nonlocal effects due to the long-range part of the Coulomb interaction are shown in the wave-vector dispersion of the magnetoplasmon modes. The Coulomb coupling between the modes is responsible for the anti-crossing. The global square-lattice symmetry is retained, whereas the local circular symmetry for a single ring is lost. This is evidenced in the periodic nature of the

wave-vector dispersions in both the x and y directions. When the excitation energy is plotted as a function of the lattice constant, the competition between the screening and the modification of the areal electron density is demonstrated. The excitation energy as a function of the radius of the ring shows two distinct regimes. The single-particle kinetic energy dominates the Coulomb interaction between electrons in the small R regime. The oscillations of the excitation energy occurring for large values of R are due to the magnetic flux quantization.

In this paper, we confined our attention to thin rings, where the electron radial motion is effectively frozen out. In the wide-ring limit, the quantization energy for radial and angular motions is comparable. Therefore, we expect the coupling between the electron radial and angular motions would be strong. This gives the anticrossing between the cyclotron and edge modes. Also, in this limit, the screening function should depend sensitively on magnetic field when the radial electron motion is included. Also, the magnetic switch of the highest occupied state obtained for thin rings will not apply to wide rings. As a matter of fact, the single-particle energy spectrum is quite different. The existence of two edges in a wide ring introduces scattering along the edges. This gives the edge-magnetoplasmon modes in this system which is fa-

vored by a low magnetic field. At high magnetic field, these edge modes will be effectively suppressed, leaving only the cyclotron modes. Calculations for wide rings are in progress.

Successful fabrication of the 2D square arrays of quantum dots and antidots (hole punching) has been reported recently.^{12,13} If one could further punch a hole at the center of each quantum dot in this 2D square array, we will obtain a quantum ring array which is proposed in this paper. Using conventional far-infrared optical absorption techniques in the presence of an external magnetic field perpendicular to the array, as used in the study of quantum dot arrays,¹² we expect to see some features predicted in this paper. Although there is still some difficulty at the present time in the fabrication of materials with the geometry discussed here, we hope that this work will stimulate experimental work which would study non-local perimeter magnetoplasmon excitations in a planar array of quantum rings.

ACKNOWLEDGMENT

This work was supported in part by a grant from the Natural Sciences and Engineering Research Council of Canada.

¹C. W. J. Beenakker, H. van Houten, and A. A. M. Staring, Phys. Rev. B **44**, 1657 (1991).

²D. Huang, Y. Zhu, Z. F. Lin, and S. X. Zhou, Phys. Rev. B **39**, 7713 (1989).

³J. K. Jain, Phys. Rev. Lett. **60**, 2074 (1988).

⁴Q. M. Li and J. Callaway, Phys. Rev. B **43**, 3278 (1991).

⁵B. J. van Wees, Phys. Rev. Lett. **66**, 2033 (1991).

⁶V. Ambegaokar and U. Eckern, Phys. Rev. Lett. **65**, 381 (1990).

⁷K. B. Efetov, Phys. Rev. Lett. **66**, 2794 (1991).

⁸G. Gumbs, D. Huang, and D. Heitmann, Phys. Rev. B **44**,

8084 (1991).

⁹A. C. Tselis and J. J. Quinn, Phys. Rev. B **29**, 3318 (1984).

¹⁰H. Ehrenreich and M. H. Cohen, Phys. Rev. **115**, 786 (1959).

¹¹S. Das Sarma and A. Madhukar, Phys. Rev. B **23**, 805 (1981).

¹²T. Demel, D. Heitmann, P. Grambow, and K. Ploog, Phys. Rev. Lett. **64**, 788 (1990).

¹³K. Kern, D. Heitmann, P. Grambow, Y. H. Zhang, and K. Ploog, Phys. Rev. Lett. **66**, 1618 (1990).